FIG. 2. Variation of modulus of rupture with Fe stoichiometry in RFe_x.

of the convoluted nature of the dendritic morphology,[4] it is highly probable that the rare-earth phase is also interconnected in the plane transverse to the growth direction. Consequently, the rare-earth phase is thought to be present as an interconnected skeleton network throughout the Terfenol-D matrix phase. The presence of a ductile skeleton network would be expected to enhance strength by retarding crack propagation throughout the brittle matrix. As X is lowered from 2.0, the volume fraction of ductile rare-earth phase increases and the strength is improved. In general, the dark microconstituent in Fig. 1 is pure rare-earth metal when its transverse dimension is small but becomes a eutectic mixture of rare-earth metal and Terfenol-D phases when its dimension increases, such as at boundary trijunctions. This eutectic mixture becomes more dominant at the lower values of X, and a reduced ductility of the eutectic mixture over the pure

rare-earth phase is probably responsible for the falloff of the slope of the strength curve in Fig. 2 at the lowest X values.

The magnetostrictive properties of Terfenol-D are only moderately reduced as X decreases from 2.0 to 1.9,[5] so that it is clearly advantageous to use values in the 1.9–1.95 range. The modulus of rupture values for X in this range are similar to typical values for glass in accord with observations that Terfenol-D deforms only elastically and is fairly brittle. However, use of X values in the 1.9–1.95 range produces a dramatic improvement in strength and elastic energy absorption, the fracture behavior is reproducible, and it is not as subject to the influence of surface finish as are some brittle materials.

[1] A. E. Clark, J. Cullen, O. McMasters, and E. Cullen, Am. Inst. Phys. Proc. 29, 192 (1976).
[2] A. E. Clark, J. P. Teters, and O. D. McMasters, J. Appl. Phys. 61, 3787 (1988).
[3] J. D. Verhoeven, A. J. Bevolo, D. T. Peterson, H. H. Baker, O. D. McMasters, and E. D. Gibson, Metallography 18, 277 (1985).
[4] J. D. Verhoeven, E. D. Gibson, O. D. McMasters, and H. H. Baker, Metall. Trans. 18A, 223 (1987).
[5] O. D. McMasters (unpublished).

Electron emission from glow-discharge cathode materials due to neon and argon ion bombardment

B. Szapiro[a] and J. J. Rocca[b]
Electrical Engineering Department, Colorado State University, Fort Collins, Colorado 80523

We have measured the electron yields of 7 glow-discharge cathode materials under bombardment by neon and argon ions with energies between 1 and 20 keV. The surfaces of the samples were conditioned by operating the materials as cold cathodes in a high-voltage glow discharge before the electron yield measurement. The materials studied are oxidized magnesium, oxidized aluminum, a molybdenum-aluminum oxide sintered composite, molybdenum, stainless steel, copper, and graphite. The dependence of electron yield on ion velocity was found to be approximately linear for all materials and gases, with the slopes being strongly material dependent. The corresponding glow-discharge current intensities were observed to have a supralinear dependence on the electron yield. The results are relevant to the design and modeling of cold cathode high-voltage glow discharges.

The phenomenon of secondary electron emission from a solid surface under ion bombardment has been studied extensively, regarding its importance in gas discharges, electron beam generation, plasma surface interactions, and ion

beam current measurements. For example, in high-voltage cold cathode glow-discharge electron guns the electron yield of cathode surfaces is a key factor in determining the electron beam current densities and generation efficiency.[1] Careful measurements of the electron yield have mostly been performed for atomically clean, flat surfaces in ultrahigh vacuum conditions.[2-7] However, these results usually do not

[a] Post-Doctoral Fellow, University of Buenos Aires.
[b] National Science Foundation Presidential Young Investigator.

apply for the operating conditions typical of high-voltage glow discharges, where sputtering effects, presence of oxide layers, and gas loading of the cold cathode surface influence the electron emissivity and thereby the discharge characteristics.

Previously, we measured the electron yields of cathode materials under helium ion bombardment for surface conditions similar to the ones present in cold cathode glow discharges.[8] Here we report the electron yields for neon and argon ion bombardment of seven cathode materials. The materials studied are oxidized magnesium, oxidized aluminum, a molybdenum-aluminum oxide sintered composite, molybdenum, stainless steel, copper, and graphite. In order to get electron yield data applicable to typical high-voltage glow-discharge cathodes the surfaces of the samples were conditioned *in situ* by operating them as cathodes of a high-voltage glow discharge in a noble gas atmosphere of the same specie that the ion beam used for the yield measurements. For aluminum and magnesium a small amount of oxygen was added to the discharge to establish a stable oxide layer, as is frequently done in high-voltage glow discharges to enhance the electron yield and decrease sputtering.[1,9-11] The temporal evolution of the conditioning discharge is monitored until a steady-state value is reached. The discharge is then interrupted, the chamber is pumped down to 10^{-6} Torr and the sample is placed on axis with an ion gun to perform the electron yield measurements. The electron yield is obtained by measuring the ion flux impinging on the cathode and the total cathode current. After the yield measurement, the discharge is reestablished and the current is monitored to verify that the surface conditions remained unchanged. The experimental setup and procedure used to perform the measurements were described in greater detail in a previous publication.[8]

The characteristics of the materials studied are similar to those used as cathodes in glow discharges: polycrystalline, commercial purity samples, machined, and polished and cleaned ultrasonically in methanol. The sintered composite was developed to be used as a high electron yield cathode material for dc electron beam glow discharges.[1] The material composition is 40% aluminum oxide and 60% molybdenum by weight, containing particles approximately 10 μm in diameter. The stainless steel is a 304 alloy.

The electron yields for neon and argon ion impact in the 1–20-keV energy range are presented in Figs. 1 and 2, respectively. At low ion energy (under 1 keV), where the potential electron emission contribution to the total yield becomes dominant, the curves should level off to a constant value; however, the energy spread of our ion beam did not allow us to accurately measure the electron yields in the low-energy range. As previously observed in the case of helium bombardment,[8] oxidized magnesium and aluminum samples
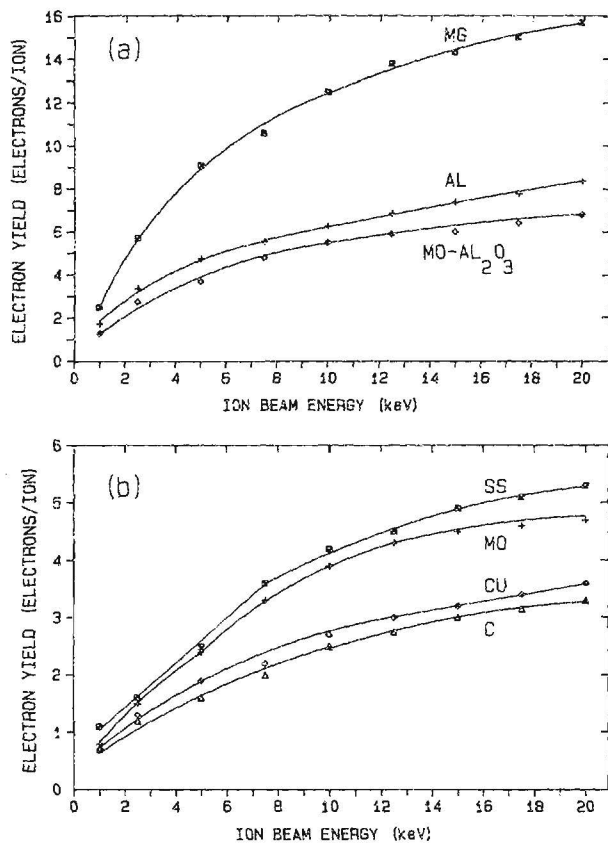

FIG. 1. Variation of the electron yield with neon ion beam energy. (a) Data for oxidized magnesium, oxidized aluminum, and a sintered composite Mo-Al$_2$O$_3$ (60%-40%). (b) Data for stainless steel, molybdenum, copper, and graphite.
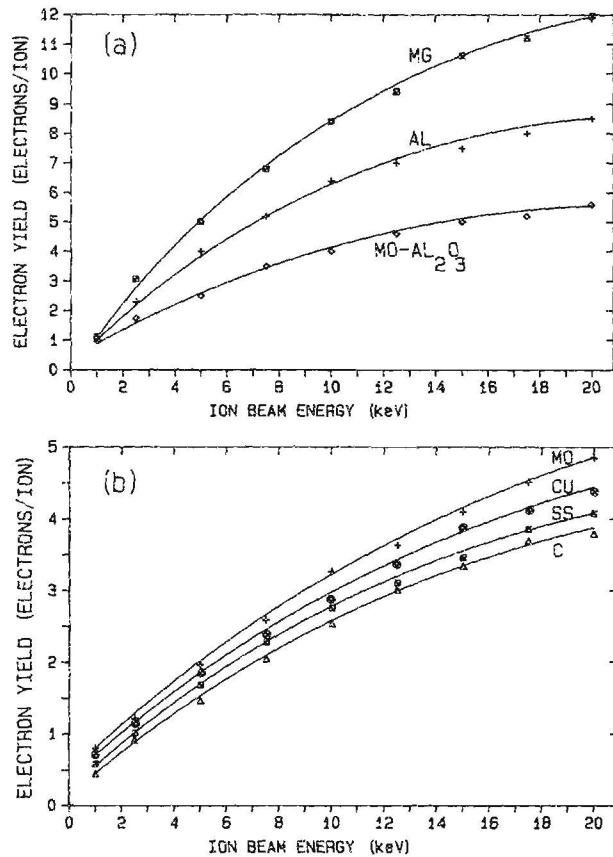

FIG. 2. Variation of the electron yield with argon ion beam energy. (a) Data for oxidized magnesium, oxidized aluminum, and a sintered composite Mo-Al$_2$O$_3$ (60%-40%). (b) Data for molybdenum, copper, stainless steel, and graphite.

B. Szapiro and J. J. Rocca

present the higher yields, followed by the sintered composite. The yields are a factor of 2–3 times higher than those measured under ultraclean conditions.[12] The increased yield in the discharged samples can be attributed to gas loading effects and increased surface roughness. Scanning electron microscope photographs of the target surface show a significant increase in surface roughness due to discharge sputtering. It should be noticed that the results of Figs. 1 and 2 might be dependent on the discharge conditions. Nevertheless, measurements obtained after discharging the cathodes under significantly discharge currents (typically a threefold increase, with current densities in the order of 10 mA/cm^2) gave yield values differing by less than 10%. Consequently, the results presented herein can be considered useful to describe conditions prevalent in many glow discharges, where the use of yields measured under ultraclean conditions of flat, elemental surfaces would in general be inappropriate.

When the data of Figs. 1 and 2 are plotted as a function of the ion velocity the dependence of the electron yields Y on this parameter is found to be approximately linear for all cathode materials and ion species. This linear increase of the yield with ion velocity has been previously observed (for instance, see Refs. 12–14) in the energy range studied. The linear dependence with velocity arises from the proportionality between Y and the electronic stopping power of the material $S_e(E_i)$ for an ion of initial energy E_i, and from the dependence $S_e \approx E_i^{1/2}$ in the energy range studied.[14] For heavy ions, the contribution by recoiling target atoms should be included[15]; nevertheless, a simple semiempirical model developed by Baragiola, Alonso, and Oliva Florio,[14] that neglects this effect, is observed to give a good description of the experimental data presented herein.

As expected, the slopes dY/dv are strongly dependent on the cathode materials and ion species, ranging from 2.6×10^{-8} electrons/(cm/s) for helium ion impact on graphite to 4.5×10^{-7} electrons/(cm/s) for argon ion bombardment on oxidized magnesium. A comparison of our molybdenum data and those obtained for flat surfaces in ultrahigh vacuum atmospheres (for instance, see Arifov, Rakhimov, and Khozinskii[12]) shows that our absolute yield values and slopes dY/dv are typically a factor of 2.5 higher, while the relative trends regarding the increase of the slopes with ion mass are similar, indicating that sputtering and gas loading effects produce an overall shift of the electron yields towards higher values.

Figures 3(a) and 3(b) illustrate the significance of the measured electron yields in determining the characteristics of glow discharges by relating the measured yields and the discharge current intensities delivered by the different materials. The data were obtained operating the samples as 1.2 cm in diameter glow-discharge cathodes by applying 2.5 kV across the discharge and a 10-kΩ ballast resistor in a neon or argon atmosphere at a pressure of 0.2 and 0.1 Torr, respectively. These pressures were selected to allow in each case generation of a high-voltage sheath in front of the cathode, and thereby bombardment of the cathode by energetic ions. The cathodes are surrounded by ceramic tubes such that electron emission occurs only from the front surface. The electron yield values used in these figures for the different
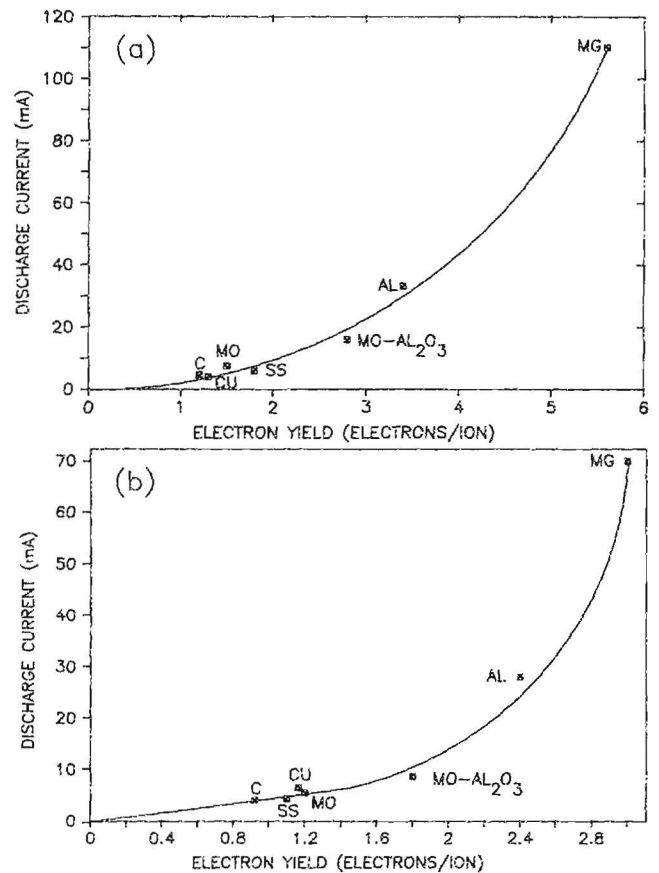

FIG. 3. Discharge current as a function of the electron yield for 2.5-keV ions. (a) Data for neon. (b) Data for argon. The cathodes are 1.2 cm in diameter. Discharge conditions are: a pressure of 0.2-Torr neon or 0.1-Torr argon (10 mTorr of oxygen added in the aluminum and magnesium cathodes), 2.5-kV voltage applied across the discharge and a 10-kΩ ballast resistor.

materials are those measured for a 2.5-keV ion beam energy. A similar supralinear glow-discharge current dependence on cathode electron yield was previously observed for helium ion bombardment and discussed in Ref. 8. The sharp increase of the discharge current with the increase in cathode electron yield indicates the importance of selecting materials with high secondary electron emission coefficient, such as oxidized magnesium or oxidized aluminum, in the design of high-current cold cathode glow discharges.

[1] J. J. Rocca, J. D. Meyer, M. R. Farrell, and G. J. Collins, J. Appl. Phys. 56, 790 (1984).
[2] M. Kaminski, Atomic and Ionic Impact Phenomena on Metal Surfaces (Springer, Berlin, 1965).
[3] G. Carter and J. S. Colligon, Ion Bombardment of Solids (Heinemann, London, 1968).
[4] D. B. Medved and Y. E. Strausser, Adv. Electron. Electron Phys. 21, 101 (1965).
[5] U. A. Arifov, Interaction of Atomic Particles With a Solid Surface (Consultants Bureau, New York, 1969).
[6] P. M. McCracken, Rep. Prog. Phys. 38, 241 (1975).

[7]K. H. Krebs, Vacuum 33, 555 (1983).

[8]B. Szapiro, J. J. Rocca, and T. Prabhuram, Appl. Phys. Lett. 53, 358 (1988).

[9]R. E. Hurley and J. H. Hollyday, Vacuum 28, 453 (1978).

[10]B. Wernsman, H. F. Ranea Sandoval, J. J. Rocca, and H. Mancini, IEEE Trans. Plasma Sci. PS-14, 4, 518 (1986).

[11]H. F. Ranea Sandoval, N. Reesor, B. Szapiro, C. Murray, and J. J. Rocca,

IEEE Trans. Plasma Sci. PS-15, 4, 361 (1987).

[12]U. A. Arifov, R. R. Rakhimov, and O. V. Khozinskii, Bull. Acad. Sci. (USSR) Phys. Ser. 26, 1422 (1963).

[13]V. G. Tel'kovskii, Dokl. Akad. Nauk SSR 20, 1079 (1956).

[14]R. A. Baragiola, E. V. Alonso, and A. Oliva Florio, Phys. Rev. B 19, 121 (1979).

[15]J. Schou, Phys. Rev. B 22, 2141 (1980).

High-power, diffraction-limited-beam operation from interferometric, phase-locked arrays of AlGaAs/GaAs diode lasers

D. Botez, L. J. Mawst, P. Hayashida, and T. J. Roth

TRW Space & Technology Group, One Space Park, M5/1065, Redondo Beach, California 90278

10/11-element interferometric phase-locked arrays with optimized facet coatings operate in array mode $L = 8$, diffraction limited to 200 mW at 2.7 times threshold, and in beam patterns 1.4 times the diffraction limit to 290 mW at 4.3 times threshold. Unlike Y-junction-coupled arrays, the beam pattern quality is not sensitive to the facet(s) reflectivity value(s). Transformation to a single-lobe pattern requires a simple phase-corrector coating or plate. The device beam pattern as a function of the array geometry is discussed.

Thompson and Whiteaway[1] have shown theoretically that high-order modes of evanescently coupled arrays are stable against gain spatial hole burning. We have reported[2] that a 10/11-element interferometric array, that selects operation in mode $L = 8$, provides diffraction-limited-beam patterns to ~85 mW and ~3 times threshold. Here we report on achieving 200 mW in a diffraction-limited-beam pattern, which, to the best of our knowledge, is the highest diffraction-limited power reported to date from 10-element phase-locked index-guided arrays. Furthermore, the results demonstrate that, unlike Y-junction coupled arrays,[3] the use of antireflection coatings on the emitting facets of evanescent-wave coupled, interferometric arrays does not affect their beam pattern.

The fundamental mode of evanescently coupled arrays invariably broadens at output powers $\geqslant 40$ mW[4] or $1.5 \times$ threshold,[4,5] due to gain spatial hole burning.[1] Previously published work on evanescent-wave coupled arrays operating in a high-order mode,[6] with optimized facet coatings, displays diffraction-limited beam operation to only 50 mW and $1.5 \times$ threshold, most probably due to weak discrimination against adjacent array modes. Y-junction coupled devices, while operating in stable fundamental-mode-like patterns, have beamwidth 3.5–4 times wider than the diffraction limit.[7] The overall interelement coupling is weak enough in Y-junction coupled devices, that their performance is highly sensitive to the feedback provided by the mirrors. Thus, when a low-reflectivity coating (3%) is applied on one facet, the lobe beamwidth increases to six times the diffraction limit,[3] due to weakened overall interelement coupling.

The interferometric arrays we report on have a similar structure to that reported on before[2]: longitudinally the device is of the wide-waveguide interferometric (WWI) type; while the cross section is very similar to that shown in Fig. 1. Previously, we reported only on arrays of 4-μm-period and 2-μm-wide elements (Fig. 1), while this paper reports on devices of both 4- and 5-μm periods, and element widths varying in the 2–4 μm range. An $Al_{0.10}Ga_{0.90}As$ antimeltback layer (0.7 μm thick) is initially grown by metalorganic vapor-phase epitaxy (MOVPE) above the substrate. The WWI pattern is etched through the antimeltback layer into the substrate, and then the rest of the structure is grown by liquid-phase epitaxy. The p-$Al_{0.30}Ga_{0.70}As$ layer is ~0.30 μm thick in between elements. 42-μm-wide SiO_2-defined metallic contact stripes are placed on the device n side to provide current confinement. One facet is coated with a six-layer dielectric stack (Al_2O_3/Si) reflector that provides 95% reflectivity at $\lambda = 0.87$ μm. The other facet is coated
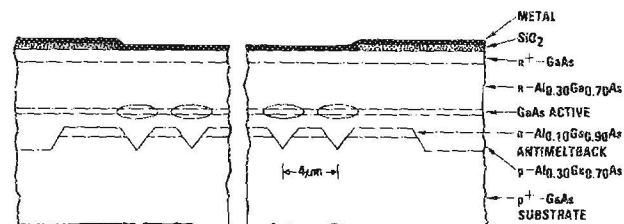

FIG. 1. Schematic respresentation of the emitting facet of the 10/11-element array. Longitudinally the device has the wide-waveguide interferometric (WWI) geometry [see Fig. 1(a) in Ref. 2].

0021-8979/89/093716-03$02.40